Journal of Inorganic and Organometallic Polymers and Materials
https://doi.org/10.1007/s10904-018-01071-2

Stable Colloidal Copper Nanoparticles Functionalized with Siloxane Groups and Their Microbicidal Activity

Estanislao Porta[1] · Sebastián Cogliati[2] · Marcos Francisco[2] · María Virginia Roldán[1] · Nadia Mamana[1] · Roberto Grau[2] · Nora Pellegri[1]

Received: 29 November 2018 / Accepted: 31 December 2018
© Springer Science+Business Media, LLC, part of Springer Nature 2019

Abstract
The emergence and spread of pathogenic microbes with resistance to multiple antibiotics necessitates the development of new broad-spectrum microbicides. Metal nanoparticles are one such microbicide and they have been recognized for their potential value in fighting harmful microbes. In this work, we show the preparation and antimicrobial characterization of copper nanoparticles, with a small percentage of copper (I) oxide, synthesized by a chemical method based on a bottom-up approach in a nonaqueous medium. In particular, we developed a new route to stabilize the copper nanoparticles, synthesized in ethanol, using an aminosilane as a capping agent. The particles were later centrifuged and suspended in ethylene glycol. The morphology, structure and stability of the Cu-APTMS NPs were characterized by UV–Vis and FTIR spectroscopy, TEM, AFM and GI-XRD techniques. The presence of colloidal nanoparticles was found 4 months after synthesization and a characteristic absorption LSPR band was registered in the UV–Vis spectrum. The Cu-APTMS NPs showed a significant in vitro degradation activity against bacterial DNA, which is important in vivo microbicidal activity. The Cu-APTMS NPs showed a strong bactericidal effect against planktonic forms of Gram-negative (*Pseudomonas aeruginosa* and enterohemorrhagic *Escherichia coli*) and Gram-positive (*Staphylococcus aureus* and *Listeria monocytogenes*) bacteria. This bactericidal effect was also observed to severely limit the viability and germination proficiency of spores of the food-poisoning and gas-gangrene producer *Clostridium perfringens*. In addition, pathogenic fungi (*Candida tropicalis* and *Fusarium verticillioides*) were irreversibly deactivated by treatment with Cu-APTMS NPs.

Keywords Copper · Nanoparticles · Siloxanes · Microbicide · Sporicide

1 Introduction

In the last decades, metallic particles of nanometric sizes have interested for the scientific community greatly due to their distinctive properties, such as high conductivity and increased chemical reactivity, which are very different from those present in the bulk material. These properties can be exploited with applications in energy [1], microelectronics [2], sensors [3], SERS [4], catalysis [5, 6], and microbiology [7]. This results in devices that have better characteristics than those found in currently available technology. Besides, noble metal nanoparticles show distinctive absorption peaks in their UV–Vis spectra, a phenomenon called Localized Surface Plasmon Resonance (LSPR). This unique optical behavior makes the nanoparticles very useful for optical applications. Many examples of devices based on Ag and Au nanoparticles can be found in the literature and several applications based on Cu nanoparticles, although to a lesser extent, have been reported recently [8–14]. This is mainly due to the difficulty of obtaining pure copper nanoparticles because of their instability with respect to oxidation under normal environmental conditions. Also, another problem of these systems is that they experience leaching [15].

Estanislao Porta and Sebastián Cogliati contributed equally to this work.

✉ Roberto Grau
robertograu@fulbrightmail.org

✉ Nora Pellegri
pellegri@fceia.unr.edu.ar

[1] Laboratorio Materiales Cerámicos, Instituto de Física Rosario, Universidad Nacional de Rosario, CONICET, 2000 Rosario, Argentina

[2] Laboratorio de Microbiología Molecular, FBioyF, Universidad Nacional de Rosario, CONICET, 2000 Rosario, Argentina

Published online: 25 January 2019

However, the use of Cu nanoparticles is of great interest since the precursors for their production are more abundant and their synthesis is cheaper, thus they are more convenient for industrial applications. Interesting examples of Cu nanoparticle synthesis and their properties can be found in both the areas of catalysis [16] and microbiology [14, 17–24].

The development of nanomaterials of low cost and low toxicity but with strong and broad microbicidal activities has attracted the attention of the scientific community as well as the industrial sectors [25–27]. Such interest arises from the ability of microbes to rapidly adapt and evolve in the presence of antimicrobial compounds. In addition, the excessive usage of traditional antibiotics in medicine, veterinary practice and animal nutrition has given rise to an abrupt increase of multidrug resistance in many microbes as well as bacteria and fungi [28, 29]. These aspects are leading to the failure of traditional antimicrobial therapy in controlling certain infectious diseases, which presents a serious concern in the health care community [30–34]. Therefore, many strategies are being used to develop new compounds with effective antimicrobial activity [35–37]. There are several mechanisms reported for antibiotic resistance: inactivation of the drug (for example, antibiotic methylation, phosphorylation, acetylation, hydrolysis, etc.); inhibition of antibiotic internalization (for example mutations or changes in porins or transporters) or activation of efflux systems; modification or change in the antibiotic target; among others [31, 32, 34, 38–41]. Moreover, the same microbial isolate (either a bacterium or a fungus) can express a simultaneous resistance to various types of antimicrobials. These multiresistant isolates—or superbugs—render standard medical therapies ineffective [32, 34, 42]. In this respect, when compared to conventional antimicrobials, nanomaterials are a promising alternative given that they have the property of avoiding the rapid emergence of resistance, amongst other advantages. The avoidance of a rapid rise in microbial resistance is because nanomaterials produce pleiotropic effects on microbes, including direct detrimental effects on microbial DNA, membrane potential, membrane protein activities and the generation of reactive oxygen species [43–46]. Antimicrobial activity of Cu NPs is clearly established, but the exact mechanisms still raise many questions. The different antimicrobial mechanisms of action of Cu NPs includes membrane damage, inhibition of respiration and protein inactivation and DNA degradation. In a recent review about antimicrobial properties of copper, Vincent et al. [47] concluded that the most interesting common point of the literature is that all bacteria exposed to copper provide survival systems only for a few minutes before undergoing cell death. No complete resistance to survive in prolonged exposure with copper has been found. Another typical issue mentioned by several researches is the ratio between the particle size and its microbicidal activity, and it has been concluded that the smaller nanoparticles are the most efficient ones. While the efficiency of copper nanoparticles as microbicides has been widely studied, and several discussions regarding the mechanism of action can be found in the existent literature, researches on using the nanoparticles in everyday life are not easily found. Recently, Palza et al. [48] showed that the total viable microorganisms amount was reduced by approximately 73% in plastic waiting room chairs when they were embedded with copper nanoparticles.

At present, and due to promising results, there is a great deal of interest in obtaining Cu nanoparticles that are stable over time [18–24]. For this purpose, different strategies have been reported, including the use of stabilizers and the anchoring of the nanoparticles on solid substrates [13]. Techniques to synthesize Cu nanoparticles include chemical reduction [49], biological methods using bacteria or leaf extracts [50–52], microwave assisted synthesis [53], ionic liquid [54], electrochemical [55], sonochemical [56], photochemical [57] and reverse-micelle [58, 59] techniques, among others. Chemical reduction is an interesting technique due to the low cost and simplicity of both the processes that take place as well as the required equipment. This method involves the reduction of a precursor salt and the use of a capping agent. Several techniques that use $NaBH_4$ in aqueous media [60–62], and also some non-aqueous synthesis have been reported, although to a lesser extent [63, 64]. While the reducing agent is important to allow the formation of metallic copper, the capping agent plays a fundamental role because it bonds to the surface of the nanoparticle, delimiting the size, contributing to the colloidal stability and granting the nanoparticles different properties depending on the characteristics of the chemical compound. There are many examples of synthesis that uses polymers as protecting agents to avoid oxidation and aggregation of Cu NPs. However, this strategy restrain the surface activity because the active sites of the particles are blocked by heavy polymer chains [65]. On the other hand, the research community made efforts to introduce the use of leaf extracts as capping and/or reducing agents to obtain Cu NPs with success [52], adding also extra activities (antioxidant, anti-allergy, antimicrobial, anti-inflammatory properties, etc.) [53]. However, when NPs are obtained for technological devices or applications, the use of a capping agent with a known composition is more adequate to introduce specific functional groups.

In this work, we present a chemical synthesis of copper nanoparticles using an aminosilane (APTMS) as a capping agent and as the precursor of siloxane groups which will act as surface modifiers. To our knowledge, no research on APTMS capped copper nanoparticles has been reported, which is why we present it here as an original technique. In this case, functionalization with the organic ligand APTMS has multiple purposes [66]. Firstly, it allows the control of the size by adsorption on the metal surface during the

synthesis, thus constituting a steric hindrance that inhibits the growth of the nanoparticles. Secondly, it contributes to the colloidal stabilization from elastic-steric interactions, solvation and osmotic repulsion. Lastly, it introduces the functional group –Si–OR which involves surface functionalization to make it vitreophilic [67]. This is useful for integrating these nanoparticles into a Sol–gel process, allowing the development of new materials, as reported for other metallic NPs [68, 69]. Siloxane groups can undergo hydrolysis and condensation reactions, which allow the formation of chemical bonds between the nanoparticles and the oxide matrices obtained via Sol–gel methods, such as SiO_2 or TiO_2 thin films. The latter has a well-known photocatalytical behavior under UV radiation. Doping the oxide matrices with Cu NPs, which have an absorption band in the visible part of the spectrum, would produce composite materials with enhanced photocatalytic properties due the action of several mechanisms including the extension of the range of use of light from solar radiation. Thus, improving the performance of these multifunctional materials [70]. Furthermore, Zhu et al. [71] have proven that an aminosilane surface coating does not induce cytotoxicity in mammalian cells, which make these aminosilanes promising compounds for microbicidal applications. In the current research, we report the bactericidal activity of the developed aminosilane capped copper nanoparticles (Cu-APTMS NPs) against Gram-positive and Gram-negative human pathogens of relevant concern plus the sporicidal and fungicidal activity against spore-forming pathogenic clostridia and fungi.

2 Experimental Section

2.1 Obtaining Stable Cu-APTMS NPs

A synthesis technique was developed to produce copper nanoparticles as described above, where the aminosilane 3-aminopropyltrimethoxysilane (APTMS, Sigma-Aldrich) was used as surface modifier. Initially, a solution of copper (II) acetate ($Cu(CH_3COO)_2$, Sigma-Aldrich) in ethanol at 24 mM was prepared. An aliquote of 165 mL of this solution was placed in a closed flask under a N_2 atmosphere, with magnetic stirring at room temperature. Then, 25 mL of a solution of the surface modifier (APTMS) in ethanol at 0.25 M was added with a syringe to avoid opening the flask. After stirring for 30 min, 10 mL of a sodium borohydride ($NaBH_4$, Sigma-Aldrich) solution in ethanol at 0.8 M was quickly added. The final concentration was $[Cu^{2+}] = 20$ mM and the ratio between the compounds was $[Cu(CH_3COO)_2]$:[APTMS]:$[NaBH_4] = 1:1.84:5$. Different colors were observed during the synthesis after the addition of $NaBH_4$, indicating the reaction progress. A study of the evolution of UV–Vis spectra during the synthesis was performed using a Jasco V-530 spectrophotometer, at different reaction times. The sample was diluted to 1 mM in ethanol and measured using ethanol as a reference in quartz cuvettes with a 1 cm optical length. This study revealed that after 4 h the spectrum did not change any more. At that point, a purification step to obtain stable nanoparticles was performed, and the colloidal nanoparticles were centrifuged at 4000 RPM for 15 min at room temperature. The supernatant was discarded and the precipitate was suspended in a solvent (either ethanol or ethylene glycol) in order to obtain the Cu-APTMS NPs suspensions at a concentration equal to 5.0 mg/mL.

2.2 Characterization of Cu-APTMS NPs

The nanoparticle characterization was performed by different techniques. An atomic force microscope (AFM) was used to study the morphologic characteristics of the nanoparticles. The samples were prepared by dropwise addition, onto a silicon (100) wafer, of the particles centrifuged and suspended in ethylene glycol and allowing the solvent to evaporate in air on a hot plate. The AFM images were obtained in air at room temperature using NanoTec Electronic equipment in a tapping mode configuration. A Si_3N_4 tip supported by a silicon cantilever (7.4 N/m spring constant and 150 kHz resonance frequency) was used. Furthermore, transmission electron microscopy (TEM) images were taken. The sample was prepared by dropwise addition of the nanoparticles, which had been centrifuged and suspended in ethanol, onto a carbon coated copper TEM grid. The studies were conducted with a Phillips EM300 microscope at 100 keV. The digital images were processed analyzed with the open source ImageJ software. To determine the crystalline structure of the NPs, grazing incidence X-ray diffraction patterns (GI-XRD) were obtained using a Philips X'Pert Pro MPD using the CuK α line. Measurements were performed using a grazing angle configuration, with an incidence angle of 5°, an increment of 0.1° and a counting time of 10 s/step. The sample was prepared by dropwise addition of the Cu-APTMS NPs which had been centrifuged and suspended in ethylene glycol onto Si (100) wafers, allowing the solvent to evaporate in air on a hot plate. In order to characterize the surface functionalization of the NPs, Fourier Transform Infrared (FTIR) spectra of the samples were performed using a Perkin Elmer Spectrum One spectrophotometer. The samples were prepared by adding one drop of the solution of Cu-APTMS NPs centrifuged and suspended in ethanol onto a Si wafer. APTMS and copper acetate FTIR spectra were obtained as references for comparison. The aminosilane sample was prepared in the same way as the Cu-APTMS NPs samples, whereas for copper acetate a small amount of the salt was mixed with KBr to form a pellet. Also, zeta potential measurements were performed in a Horiba SZ-100 nanoparticle analyzer equipment for both Cu-APTMS NPs

suspensions in ethanol and in ethylene glycol at a concentration equal to 0.5 mM. Stability characterization was performed by measuring UV–Vis spectra of the Cu-APTMS NPs suspensions during the following days after the synthesis was finished.

2.3 Microbiological Studies

2.3.1 Strains and Growth Conditions

Seven different bacterial strains and two fungal isolates (Table 1) were used to study the antimicrobial activity of the Cu-APTMS NPs. Two of the bacterial strains used were representative of spore-forming bacteria: the reference *Bacillus subtilis* NCIB3610 strain and the pathogenic enterotoxin-positive and gas gangrene producing *Clostridium perfringens* SM101 strain [66]. The other five bacterial strains were the ampicillin-resistant enterohemorrhagic *Escherichia coli* (EHEC) strain O157:H7, the hemmolysin-positive *Listeria monocytogenes* strain ATCC 7644, a human-blood isolated methicillin-resistant *Staphylococcus aureus* strain, the cause of life-threating infections *Pseudomonas aeruginosa* PAO-1 strain and the non-pathogenic laboratory *E. coli* strain DH5α. The fungi studied were the opportunistic human pathogens *Candida tropicalis* and *Fusarium verticillioides*. All microbes were grown in a Luria–Bertani broth (LB, Difco Co.) under aerobic conditions with the exception of the *C. perfringens* SM101 strain, which was grown in a BHI (Brain Heart Infusion) medium under anaerobic conditions in anaerobic jars containing Gas Packs (BD Biosciences, USA) at 37 °C. To get spores, *B. subtilis* cells were grown in the Schaeffer's sporulation medium (SM) under aerobic conditions at 37 °C [72] and *C. perfringens* was grown in the Duncan Strong sporulation medium (DSSM) under anaerobic conditions at 37 °C as previously described [73]. After the reported times, the bacilli and clostridia cultures were treated at 80 °C for 15 min. This temperature treatment irreversibly inactivated (killed) vegetative bacteria while spores remained viable [72].

2.3.2 Degradative Effect on Bacterial DNA

The DNA cleavage efficiency of the Cu-APTMS NPs was measured by determining their ability to convert the supercoiled DNA form of the bacterial plasmid pHT315 [72, 74] to the nicked and linear forms, and further degradation. Plasmid DNA was purified from a pHT315-harboring DH5α strain [72] using a miniprep purification kit (Wizard-Promega Co). Reactions contained aliquots of 3 µg of pHT315 incubated at 37 °C in the presence of Cu-APTMS NPs at the different indicated concentrations. The incubations were stopped by the addition of 5 µL of loading buffer (0.25% w/v bromophenol blue and 30% v/v glycerol in water) and keep at − 20 °C until used. The products resulting from interactions of the Cu-APTMS NPs with DNA were separated by electrophoresis on agarose gels (1% w/v), which contained 1 µg/mL ethidium bromide, 20 mM sodium acetate, 2 mM Na_2EDTA, pH 7.5, at 5 Vcm^{-1}. Agarose gel electrophoresis was performed in a horizontal gel apparatus (Mini-SubTM DNA Cell, BioRad Co) for about 4 h and gels were visualized and photographed under an UV transilluminator [73].

Table 1 Microbial strains used in this work and their main characteristics

Microorganism	Strain	Type of microbe[a]	Associated disease	Main antimicrobial resistance
Bacillus subtilis	NCIB3610[b]	G(+) bacteria	None	None
Clostridium perfringens	SM101	G(+) bacteria	Gas gangrene, enteritis necroticans, food poisoning and antibiotic-associated diarrhea	Chloramphenicol
Staphylococcus aureus	ST239	G(+) bacteria	Bacteremia and infective endocarditis, skin and soft tissue infections, bone and joint infections, pneumonia, food poisoning	β-lactams (methicillin)[c]
Listeria monocytogenes	ATCC7644	G(+) bacteria	Listeriosis and febrile gastroenteritis	Penicillins and cephalosporins[c]
Escherichia coli	DH5α	G(−) bacteria	None	Ampicilin
Enterohemorrhagic *Escherichia coli* (EHEC)	O157:H7	G(−) bacteria	Bloody diarrhea and hemolytic uremic syndrome	β-lactams[c]
Pseudomonas aeruginosa	PAO-1	G(−) bacteria	Life-threating infections of lungs and airways (pneumonia), urinary tract and wounds	β-lactams[c]
Candida tropicalis	Clinical isolate	Yeast	Bronchomycosis and vaginosis	Fluconozole
Fusarium verticillioides	ATCC3629	Filamentous fungi	Allergic diseases (sinusitis) and mycotoxicosis	Itraconazole, voriconazole

[a]G(+): Gram-positive, G(−): Gram-negative

[b]Spore-forming reference strain

[c]ESBL: Extended spectrum β-lactamases

2.3.3 Bactericidal Activity Assays

Ten milliliters of LB broth containing an average number of 1×10^8 and 1×10^7 colony forming units (CFU) per mL of bacteria or fungi, respectively, were co-cultivated with Cu-APTMS NPs or Cu_2O (cuprous oxide, Sigma Aldrich), suspended in ethylene glycol, as a control at the indicated concentrations. The growth temperature was 37 °C or 28 °C for bacteria and fungi, respectively. The microbicidal effect of Cu-APTMS NPs against the growth of planktonic cultures was quantified, after 16 h or 36 h of growth again for the treated bacteria and fungi, respectively. After these incubation times, we performed serial dilutions of the microbial cultures in sterile water, and plated them on LB agar Petri dishes for 48 h before counting the colony forming units (CFU). The minimal inhibitory concentration (MIC), in µg/mL, is defined as the lowest concentration of a compound (Cu-APTMS or Cu_2O) that inhibits the growth of the microorganism as evaluated by a culture absorbance lower than 0.05 (Optical Density at 600 nm). The minimal microbicidal concentration (MMC), in µg/mL, is defined as the drug concentration which completely inhibited the bacterial survival (counting of CFU lower than ten per milliliter).

2.3.4 Sporicidal Activity Assays

For the evaluation of the sporicidal activity, 10 mL of pure spores of *B. subtilis* and *C. perfringens* (as evaluated by the spore refractability under observation by phase contrast microscopy and heat resistance) [75] were centrifuged (5 min at 4,500 rpm) and concentrated at a final titer of 1.5×10^9 spores/mL. These spore preparations were placed in contact with Cu-APTMS NPs prepared at different concentrations as indicated and incubated at room temperature for 4 h. After these incubations, appropriate aliquots were taken and diluted before counting on LB agar plates under aerobic conditions or BHI agar plates under anaerobic conditions for *B. subtilis* and *C. perfringens*, respectively, as indicated.

2.3.5 Spore Germination Assays

Pure spore solutions of *B. subtilis* or *C. perfringens* were concentrated until reaching an OD_{600nm} ~ 1.0 (2.0×10^9 spores/mL). Then, one milliliter of these spore suspensions of *B. subtilis* or *C. perfringens* were incubated, in PBS buffer with 100 µL of AFGK germinant solution (10 mM L-asparagine, 100 mM D-glucose, 100 mM D-fructose, 100 mM KCl), to evaluate spore germination proficiency [75] in the absence or presence of microbicides (Cu-APTMS NPs or Cu_2O) at a concentration of 20 µg/mL. Spore germination was measured at room temperature by monitoring the decrease of the OD_{600nm} levels (because of the release of dipicolinic acid) over time [76]. Levels of spore germination were confirmed by the loss of spore refractability as analyzed by phase-contrast microscopy at the end of the experiments. The experiments were performed in triplicate.

3 Results and Discussion

3.1 Synthesis of Cu-APTMS NPs

Cu-APTMS NPs were obtained by a chemical reduction technique. The synthesis was initiated by the dissolution of the copper (II) acetate in ethanol, obtaining a homogeneous light blue solution. Then, under a N_2 atmosphere, aminosilane was added to act as capping agent of metal nanoparticles. After the addition, an immediate change of color was observed, from light blue to blue, due the formation of a complex between copper (II) and APTMS [77]. The addition of the ligand APTMS also introduces modifications in the pH of the medium and consequently changes the reduction potential of the metal. These changes can influence the reaction kinetics and may show a noticeable effect on the size or morphology of the resulting nanoparticles, as reported previously by Dang et al. [49]. Zhang et al. [64] have reported previously that a pH near 11 stabilizes the copper precursor during the synthesis and achieves good size control in organic solvents. Thus, our synthesis was performed at a pH equal to 11. Finally, this produced the reduction in a short period of time, allowing rapid nucleation, $NaBH_4$ was quickly added under vigorous stirring, gradually changing the solution appearance, first to a reddish orange color and finally resulting in a black suspension. The use of an oxygen free atmosphere was very important to avoid the immediate oxidation and dissolution of the Cu-APTMS NPs formed during this stage.

UV–Vis spectra acquired at different times during the synthesis show an absorption band with a maximum near 615 nm and increasing intensity until stabilizing after 4 h (Fig. 1a). This absorption band is due to the local surface plasmon resonance (LSPR) phenomenon, caused by the interaction of metallic copper of nanometric size with light [78]. From these spectra, we confirmed that 4 h is enough time to obtain the maximum possible yield of colloidal Cu-APTMS NPs under these reaction conditions. Since this is the first time that an aminosilane of this type was used as a surface modifier for Cu-APTMS NPs, several characterization techniques were used in order to discern the morphology and structure of the material.

Information about the crystalline structure was obtained from the GI-XRD pattern acquired from powder nanoparticle samples. The GI-XRD pattern (Fig. 1b) shows three well defined, broad peaks at 43.3°, 50.5° and 74.1°, which are associated with the family planes

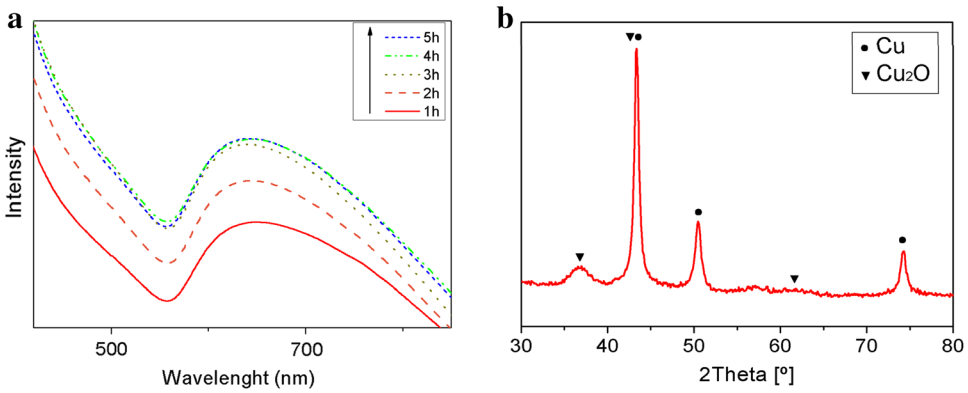

Fig. 1 **a** UV–Vis spectra of aliquots of the reaction medium to obtain Cu NPs extracted at different times during the synthesis. **b** GI-XRD pattern of Cu-APTMS NPs deposited over a Si (100) wafer

[111], [200] and [220] of the metallic copper, with a cubic Fm-3m structure (JCPDS No. 85-1326). The crystallite size calculated by the Scherrer equation was 26 nm. Additional peaks centered at 36.5°, 42.4° and 61.6° are identified, which can be associated with the family planes [111], [200] and [220] of copper (I) oxide with a cubic Pn-3m structure (JCPDS No. 78-2076). The area under the curves corresponding to the observed peaks, infers that metallic copper is more than 88% of the total copper content in the nanoparticle, according to calculations performed with the MAUD software [79]. The width of the copper (I) oxide peaks indicates that the crystal domains are in the nanometric size range, which is smaller than the Cu^0 nanostructures. The corresponding crystallite size calculated by the Scherrer equation was 4 nm. Moreover, the crystalline phases indexed by GI-XRD were also confirmed by electron diffraction using TEM (not shown here), where the Cu and Cu_2O planes are clearly identified in the ring diffraction patterns.

To determine the morphology of the NPs, TEM images were analyzed. Some of these images are shown in Fig. 2. Mostly spherical isolated nanoparticles are observed (as shown in Fig. 2a) together with some agglomerates. A statistical analysis of size distribution was performed from over 1000 particles observed in several TEM images using the ImageJ software, allowing the construction of a histogram (Fig. 2b). The results indicated a wide size distribution with an average particle size of 25 nm and a standard deviation of 19 nm. The AFM topographic images (Fig. 2c) confirm the presence of both isolated and agglomerated Cu-APTMS NPs. From the analysis of different Z profiles (an example of which is shown in Fig. 2d), it is inferred that the size of isolated Cu-APTMS NPs are in agreement with those obtained by TEM measurements. Moreover, these values also agree with the crystal size calculated from GI-XRD, indicating that the NPs are monocrystalline.

3.2 Stability of the Cu-APTMS NPs

Knowledge of the morphologic characteristic of the nanoparticles allows further understanding of the UV–Vis spectra at the different steps of the synthesis. Regarding the composition of the nanoparticles, it is known that Cu nanoparticles are highly unstable due to oxidation. The oxidation process can produce Cu^+ and Cu^{2+}, which are present as oxides or cations. So, achieving NPs stability over time is crucial and it defines the quality of a synthetic route and the relevance of the product to be used in further applications. Therefore, the stability of the colloidal nanoparticles was studied by UV–Vis spectroscopy, through analysis of the absorption by LSPR. The maximum absorption for colloidal Cu nanoparticles is between 500 and 650 nm [80]. It is notable that Cu_2O does not show absorption in this range. Thus, the analysis of the optical properties allows us to determine whether nanoparticles remain in their zero valence state.

For the Cu-APTMS NPs obtained without a purification step, an absorption maximum is located at 618 nm, corresponding to the LSPR absorption. This optical property remains stable as long as the sample is kept under N_2 atmosphere. When exposed to atmospheric room conditions, the LSPR absorption band vanishes after a few minutes (Fig. 3a). When ethanol was used to suspend the Cu-APTMS NPs after centrifugation, the UV–Vis spectrum shows a well-defined LSPR absorption band at 610 nm, which can be observed clearly for five up to days (Fig. 3b). After that period, the LSPR absorption band decreases quickly in intensity due to leaching, oxidation and dissolution processes. On the other hand, the use of ethylene glycol as the solvent after centrifugation enhances the stability of the colloidal Cu-APTMS NPs even more. Immediately, after resuspension in ethylene glycol, the LSPR absorption band with the maximum centered at 603 nm can be observed (Fig. 3c) and it is clearly distinguishable after 38 days. Moreover, it can still be observed for up to 4 months later with lesser

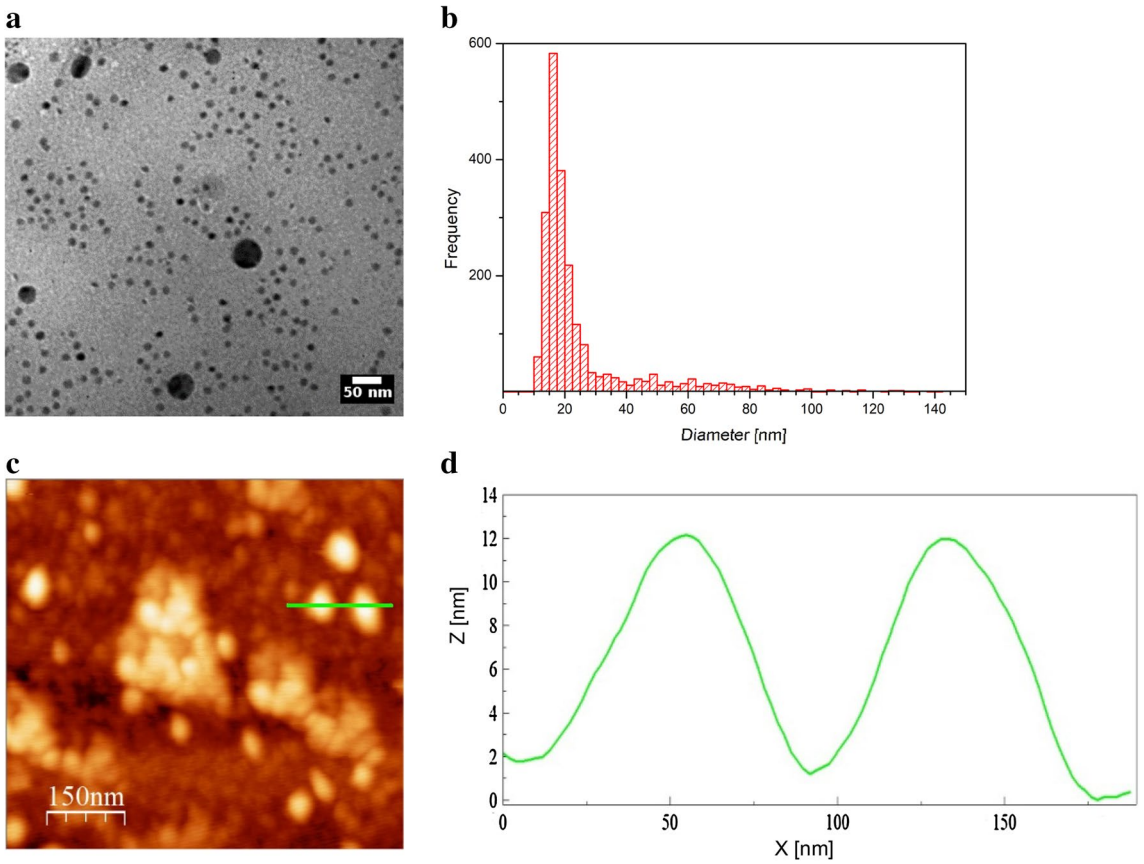

Fig. 2 **a** TEM bright field image of Cu-APTMS NPs. **b** Size distribution histogram obtained from several TEM images. **c** AFM topographic images of Cu NPs deposited over Si (100) acquired using the Tapping Mode. **d** The Z profile of the area indicated with the green horizontal line in Fig. 2d showing two isolated nanoparticles

intensity and a shift towards longer wavelengths. This is consistent with previous results regarding agglomeration. Although the intensity of the LSPR maximum in ethylene glycol diminishes over time, it fades more slowly than for the Cu-APTMS NPs in ethanol. This indicates the presence of colloidal Cu-APTMS NPs confirming that the purification process increases the stability of the nanoparticles, slowing down the dissolution process.

The colloidal stability of the suspensions in ethylene glycol is related to the electrostatic repulsion component of the colloidal stabilization. Zeta potential (ZP) measurements were carried out to obtain information about this subject. All measurements were performed at a 30.0 µg/mL concentration. For Cu-APTMS NPs without any purification process, ZP was 24 mV. After the centrifugation and suspension in ethanol, the sample ZP was 24 mV. For Cu-APTMS NPs centrifuged and suspended in ethylene glycol at a concentration of 30.0 µg/mL, the ZP was 37 mV. These results agree with the research by Bhattacharjee [81], and they indicate that Cu-APTMS NPs suspended in ethylene glycol were highly stabilized by electrostatic repulsions, making long-term colloidal stability possible.

Figure 3d shows FTIR spectrum of Cu-APTMS NPs after the purification step. Copper (II) acetate and APTMS spectra are also shown as a reference. Peaks of APTMS and copper (II) acetate absorption bands are present in the Cu-APTMS NPs spectrum, even though some differences can be seen. In the Cu-APTMS NPs spectra there is an additional peak at 1729 cm^{-1} (indicated with a vertical line in the figure), which can be attributed to C=O bond of the amide group [82]. This indicates that APTMS reacted with the acetate groups present in the medium during the synthesis, forming an amide group that makes final absorption on the surface of the nanoparticle possible. A broad absorption band at approximately 1100 cm^{-1} is observed in the APTMS spectrum due to the overlapping of two peaks at 1122 and 1077 cm^{-1} (also indicated with vertical lines in the Fig. 3d). These peaks are assigned to the anti-symmetric (ν_{as}) and symmetric (ν_s) stretching bands of Si–O–C respectively [83] and are present in the spectrum of Cu-APTMS NPs as well, indicating the effective functionalization of the particle surface with the siloxane groups.

In the APTMS spectrum, peaks associated to the anti-symmetric (ν_{as}) and symmetric (ν_s) stretching bands can be

observed at 3361 cm^{-1} and 3290 cm^{-1}, respectively. In the spectrum of Cu-APTMS NPs, a shift is observed in these peaks, resulting in absorption bands situated in 3452 cm^{-1} (ν_{as}) and 3426 cm^{-1} (ν_s). These redshifts in the primary amines FTIR absorption bands indicate that there is a strong interaction between atoms of N and Cu, which suggests that the amine groups are binded to the copper nanoparticles surface [84]. Thus, we obtained Cu NPs capped by APTMS anchored through the amine groups, whereas siloxane groups remain exposed to the reaction medium. The siloxane groups are able to react with oxide surfaces or metal alcoxides by hydrolysis (Eq. 1) and condensation (Eqs. 2 and 4), according to the following scheme:

$$NH_2(CH_2)_3Si(OCH_3)_3 + n\ H_2O \rightarrow NH_2(CH_2)_3Si(OCH_3)_{3-n}(OH)_n + n\ CH_3OH \quad (1)$$

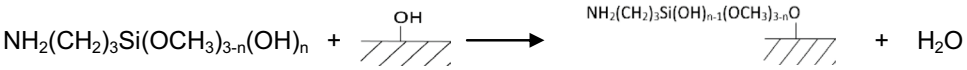

(2)

$$M(OR)_m + H_2O \rightarrow M(OR)_{m-1}(OH) + ROH \quad (3)$$

$$NH_2(CH_2)_3Si(OCH_3)_{3-n}(OH)_n + M(OR)_{m-1}(OH) \rightarrow NH_2(CH_2)_3Si(OCH_3)_{3-n}(OH)_{n-1}OM(OR)_{m-1} + H_2O \quad (4)$$

Therefore, it is possible to anchor the Cu-APTMS NPs onto an oxide surface by chemical bonds or also, to introduce them into solid matrices obtained by sol–gel techniques [85].

These overall results (Figs. 1, 2, 3) allowed us to conclude that Cu NPs stabilized by APTMS and suspended in ethylene glycol can be manipulated under ambient conditions for several days without the evolution of aggregation, precipitation or oxidation. Thus, these nanoparticles are able to be used in different technological applications including microbiology.

3.3 Antimicrobial Activity of the Cu-APTMS NPs

Previous studies showed that Cu-NPs had a potent bactericidal effect that could at least partially be explained by its detrimental activity on microbial DNA stability. In an attempt to characterize the biological activity of the Cu-APTMS NPs, before evaluating their in vivo microbicidal effects against selected microorganisms, we analyzed how Cu-APTMS NPs affected the stability of bacterial DNA. The DNA cleavage efficiency of the Cu-APTMS NPs was measured by determining their ability to convert the supercoiled and the relaxed DNA (covalently closed circular and nicked or open circular forms, respectively) to a linearized form or to further degrade the DNA [24]. To this end, purified plasmid DNA (pHT315) was treated with different concentrations of Cu-APTMS NPs (Fig. 4) for 2 h at 37 °C before separation of the DNA forms (supercoiled, relaxed and linearized) by agarose gel electrophoresis. The electrophoretic running of untreated pHT315 showed the typical three plasmid bands with a strong predominance of the covalent closed circular (supercoil) form (Fig. 4, lane 2). After treatment of pHT315 with the lower Cu-APTMS concentration (0.5 µg/mL), the supercoiled form of the plasmid completely disappeared and only the relaxed and linearized forms were observed along with the appearance of a long smearing of degraded DNA (Fig. 4, lane 4). At the highest assayed Cu-APTMS concentration (5.0 µg/mL), only a tiny band corresponding to the linearized form was observed, plus the appearance of a smear-like band corresponding to degraded DNA (Fig. 4, lane 3).

After demonstrating the biological activity of the Cu-APTMS NPs (Fig. 4), we proceed to characterize their microbicidal activity against relevant health-concern microorganisms: *P. aeruginosa* and EHEC-enterohemorrhagic *E. coli*-(Gram-negative), spore-forming *C. perfringens, S. aureus* and *L. monocytogenes* (Gram-positive), *C. tropicalis* (yeast) and *F. verticillioides* (mold), see Table 1. In addition to these pathogens, the spore-forming bacteria *B. subtilis* NCIB3610 and the *E. coli* strain DH5α were used as a control of non-pathogenic Gram-positive and Gram-negative bacteria, respectively [75, 86–90]. As shown in Fig. 5, the use of increasing concentrations of Cu-APTMS NPs produced an increased microbicidal effect that was seen in a reduction in the final titer of viable microorganisms, CFU/mL, obtained after treatment. In addition, some other interesting conclusions can be drawn from this experiment (Fig. 5). First, the active compound responsible for the microbicidal effect was the copper present in the Cu-APTMS NP preparation because the APTMS alone (in ethylene glycol) did not produce any significant microbicidal activity on the tested microorganisms. Although it is well known that the capping agent has influence over the antimicrobial activity, it is not possible to compare these results with similar bare particles due the rapid oxidation upon air exposure during aerobic conditions in antimicrobial tests. Secondly, the Cu-APTMS NPs were more efficient as microbicides

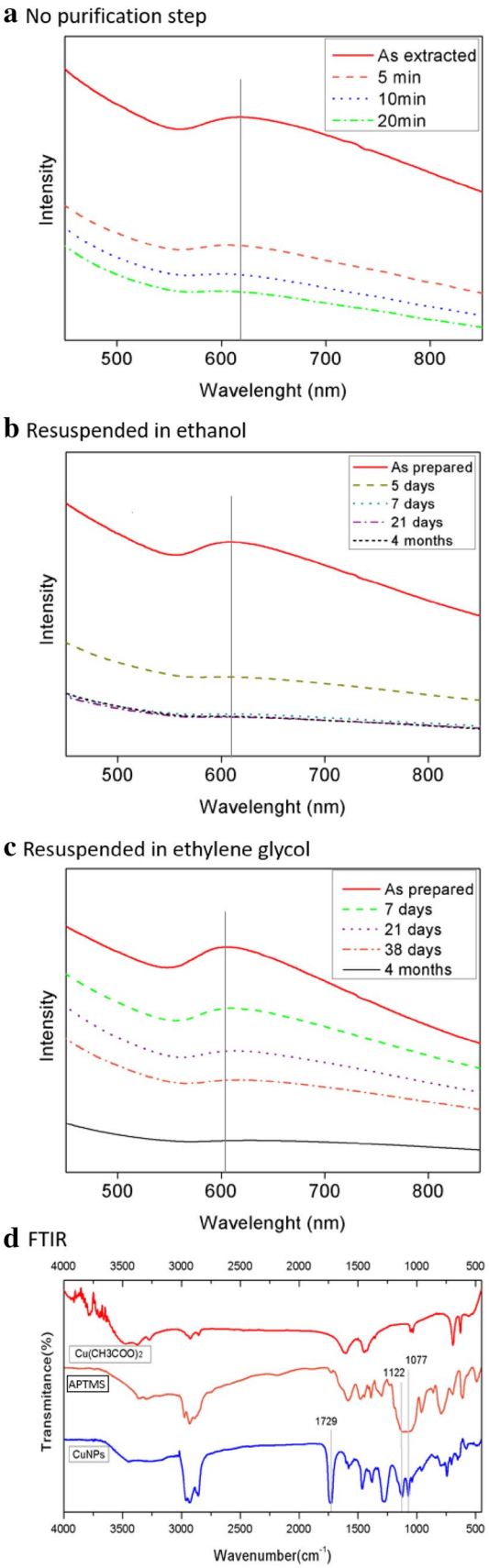

Fig. 3 UV–Vis spectra with evolution of time for the colloidal Cu-APTMS NPs kept in air. **a** NPs without any purification step. **b** NPs centrifuged and suspended in ethanol. **c** NPs centrifuged and suspended in ethylene glycol. **d** FTIR spectra of copper (II) acetate, APTMS and Cu-APTMS NPs

than cuprous oxide (Cu_2O). This result is relevant because it strongly suggests that the enhanced microbicidal effect of the Cu-APTMS NPs was due to the nanometric metallic copper. Similar results were shown in a research performed by Chatterjee et al. [91], which compares the antimicrobial activity of Cu NPs and $CuCl_2$. They attributed the cell filamentation and cell killing effects of the Cu NPs to the nascent Cu^{2+} ions, originating from the oxidation of the metallic Cu atoms of the NPs. These ions proved to be more effective as microbicides than the Cu^{2+} ions from a $CuCl_2$ solution. Another interesting observation from Fig. 5, is that the tested Gram-positive bacteria (*B. subtilis, S. aureus* and *L. monocytogenes*) were more sensitive than the tested Gram-negative pathogenic bacteria (EHEC and *P. aeruginosa*) to the microbicidal effect of the Cu-APTMS NPs. The minimal obtained microbicidal concentrations (MMC) vary from (5–20 µg/mL) and (20–30 µg/mL) for Gram-positive and Gram-negative bacteria, respectively (Fig. 5a–f; Table 2). Accordingly, the minimal inhibitory concentration (MIC)

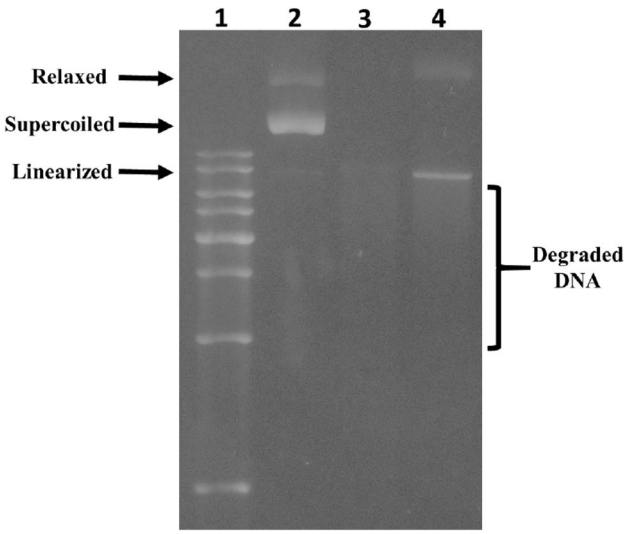

Fig. 4 Degradation of bacterial plasmid DNA by Cu-APTMS NPs. The DNA cleavage efficiency of the Cu-APTMS NPs was measured by determining their ability to convert the supercoiled (covalently closed circular) and the relaxed form of pHT315 to the linearized form or to completely degraded DNA. Reactions (lanes 3 and 4) contained 3 µg of pHT315 and Cu-APTMS NPs at 0.5 µg/L (lane 4) or 5.0 µg/L (lane 3) and were incubated at 37 °C for 2 h. Reactions were stopped by the addition of 5 µL of loading buffer, and the products resulting from interactions of the Cu-APTMS NPs with DNA were separated by agarose gel electrophoresis and photographed as indicated. Lane 1: 1 kb ladder, lane 2: 3 µg of untreated pHT315

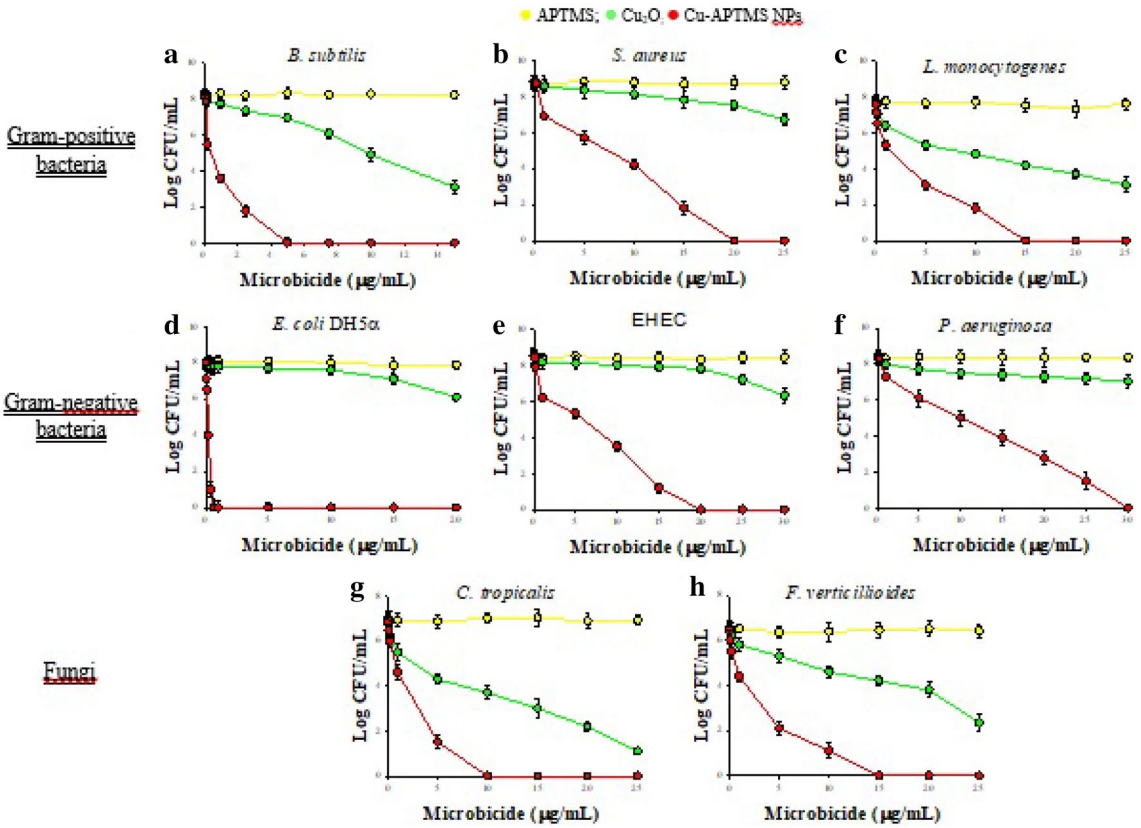

Fig. 5 Microbicidal activity of Cu-APTMS NPs against Gram-positive (**a**–**c**), Gram-negative (**d**–**f**) and fungi (**g**–**h**) microorganisms. Microbes were grown in LB broths supplemented with Cu-APTMS NPs in ethylene glycol (red circle), APTMS in ethylene glycol (yellow circle), ethylene glycol (black circle) and Cu_2O in water (green circle) at the indicated concentrations during 16 h at 37 °C or 36 h at 28 °C for bacteria and fungi, respectively. After these incubations, appropriate dilutions of each microbial culture were plated on LB agar plates and incubated for 48 h at 37 °C or 28 °C for bacteria and fungi, respectively, before colony counting (CFU) was performed. Experiments were conducted in triplicate and a typical result ± S.E.M. (Standard Error of the Mean) is shown

Table 2 Minimal inhibitory concentrations and minimal microbicidal concentrations (MIC and MMC, respectively) of Cu-APTMS and Cu_2O against Gram-positive, Gram-negative bacteria and fungi

Strain	MIC (µg/mL)		MMC (µg/mL)	
	Cu-APTMS NPs	Cu_2O	Cu-APTMS NPs	Cu_2O
B. subtilis	3.5 ± 0.2	45.0 ± 0.5	5.0 ± 0.2	45.0 ± 0.5
S. aureus	15.0 ± 0.4	> 100	20.0 ± 0.3	> 100
L. monocytogenes	12.5 ± 0.2	50.0 ± 0.70	15.0 ± 0.2	50.0 ± 0.7
EHEC	15.0 ± 0.4	> 100	20.0 ± 0.5	> 100
E. coli DH5α	0.20 ± 0.04	> 100	2.50 ± 0.03	> 100
P. aeruginosa	20.0 ± 0.5	> 100	30.0 ± 0.2	> 100
C. tropicales	7.5 ± 0.1	25.0 ± 0.5	10.0 ± 0.1	40.0 ± 0.4
F. *verticillioides*	12.0 ± 0.2	35.0 ± 0.3	15.0 ± 0.2	50.0 ± 0.3

The MIC is defined as the lowest concentration of a compound that inhibits the growth of the microorganism, and MMC is defined as the drug concentration which completely killed the microorganism. The average of three independent determinations ± S.E.M is shown

was lower for Gram-positive bacteria (3.5–15 µg/mL) than for Gram-negative bacteria (15–20 µg/mL) (Table 2). These differences in microbicidal susceptibility among Gram-positive and Gram-negative bacteria can be explained by the permeability barrier represented by the outer membrane (mainly due to the lipopolysaccharide, LPS) present in the Gram-negative bacteria. Supporting this interpretation, the DH5α strain which showed the highest sensitivity to the

Cu-APTMS NPs (MIC and MMC of 0.2 µg/mL and 2.5 µg/mL, respectively, Fig. 5d; Table 2) is a Gram-negative laboratory strain that harbors several mutations that decrease the size of its LPS, and therefore makes it more sensitive to microbicides than wild *E. coli* isolates [92]. Accordingly, the Cu-APTMS NPs were significantly more efficient as a fungicide than Cu_2O (Fig. 5g, h), and the yeast was more sensitive to the microbicidal treatments with the Cu-APTMS NPs and Cu_2O than the mold, probably due to the hyphae and mycelia barrier in the latter. Finally, and very interestingly, the Cu-APTMS NPs were more efficient microbicides at lower concentrations than other Cu NPs preparations reported in the literature [14, 17, 18, 20–24, 87–97].

Spores are the most resistant and dangerous microbial form that persist in the environment [80, 91]. Spores formed by pathogenic bacteria (mainly bacilli and clostridia) represent a serious threat against human health, not only under normal situations (for example in cases of accidental food poisoning after the consumption of uncooked meat or gas gangrene development in cases of uncontrolled mellitus diabetes) but also in case of bioterrorism [98, 99]. To our best knowledge, there are no previous reports of the susceptibility of bacterial spores to Cu-APTMS NPs [18, 93–97]. As shown in Fig. 6 the Cu-APTMS NPs exhibit a strong sporicidal effect, which is significantly greater than that produced by Cu_2O against *B. subtilis* and *C. perfringens* spores prepared at a concentration of 1×10^9 spores/mL, a spore titer similar to what could be utilized in a bioterrorist [75, 98]. The Cu-APTMS NPs were also effective in blocking spore germination, while Cu_2O was not (Fig. 7). This is an important and valuable attribute of the Cu-APTMS NPs that makes them superior to Cu_2O given that in the case of an accident or bio-attack with spores of pathogenic bacilli (i.e., *B. anthracis, B. cereus*) or clostridia (*C. perfringens, C. botulinum, C. tetani, C. difficile*, etc.), the Cu-APTMS NPs would impair their germination (i.e., the emergence of the active, vegetative, and virulent form of the pathogen) and therefore block the development of the disease (anthrax, diarrhea, gas gangrene, botulism, tetanus, and bloody diarrhea, respectively). Overall, these results (Figs. 5, 6, 7) strongly suggest the suitability of the developed Cu-APTMS NPs to irreversibly inactivate planktonic and spore forms of pathogenic bacteria and fungi.

4 Conclusions

A route for the synthesis of stable Cu nanoparticles with a small amount of copper (I) oxide (Cu_2O) and functionalized with siloxane groups was developed through a continuous medium technique. Stable, spherical and monocrystalline nanoparticles were obtained through a bottom-up method, and kept in non-aqueous colloidal suspensions. The preparations exhibited the presence of colloidal copper nanoparticles for up to 4 months in ethylene glycol. The purification step was crucial to reach the reported stability of the suspensions. An effective functionalization of the surface with

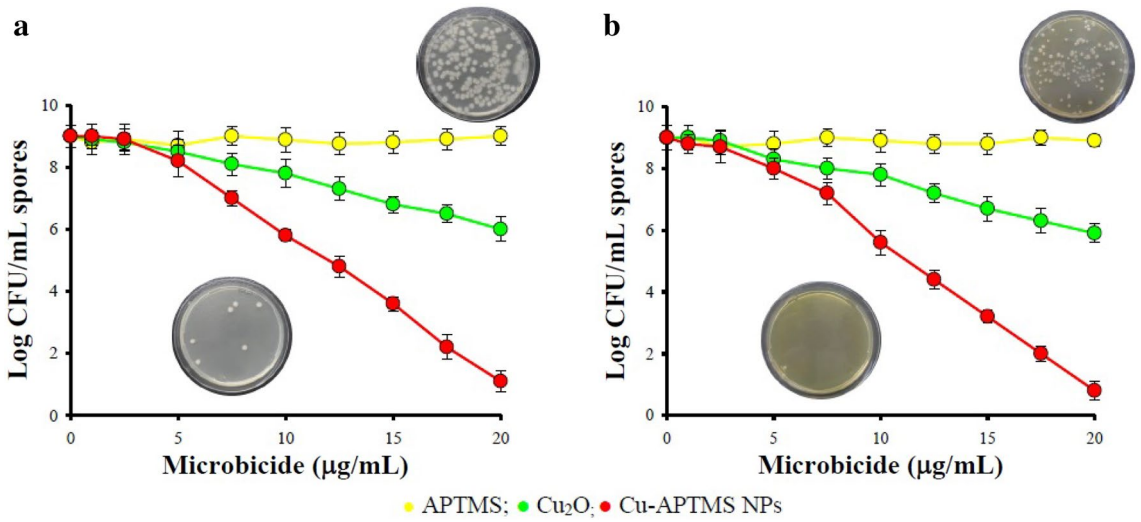

Fig. 6 Sporicidal activity of Cu-APTMS NPs against *B. subtilis* **a** and *C. perfringens* **b** spores. Cu-APTMS in ethylene glycol (red circle), APTMS in ethylene glycol (yellow circle), ethylene glycol (black circle) and Cu_2O in water (green circle) were evaluated at room temperature for 4 h at the indicated concentrations. After the 4 h appropriate dilutions were made and plated on LB agar plates under aerobic conditions or BHI agar plates under anaerobic conditions for *B. subtilis* and *C. perfringens*, respectively. These Petri dishes were incubated during 36 h at 37 °C before colony counting (CFU). Insert photographs show the CFU formed on LB or BHI plates of *B. subtilis* or *C. perfringens* spores, respectively, untreated (top pictures) or treated (bottom pictures) with the highest concentration (80 µM) of Cu-APTMS NPs. All experiments were performed in triplicate and a typical result ± S.E.M. is shown

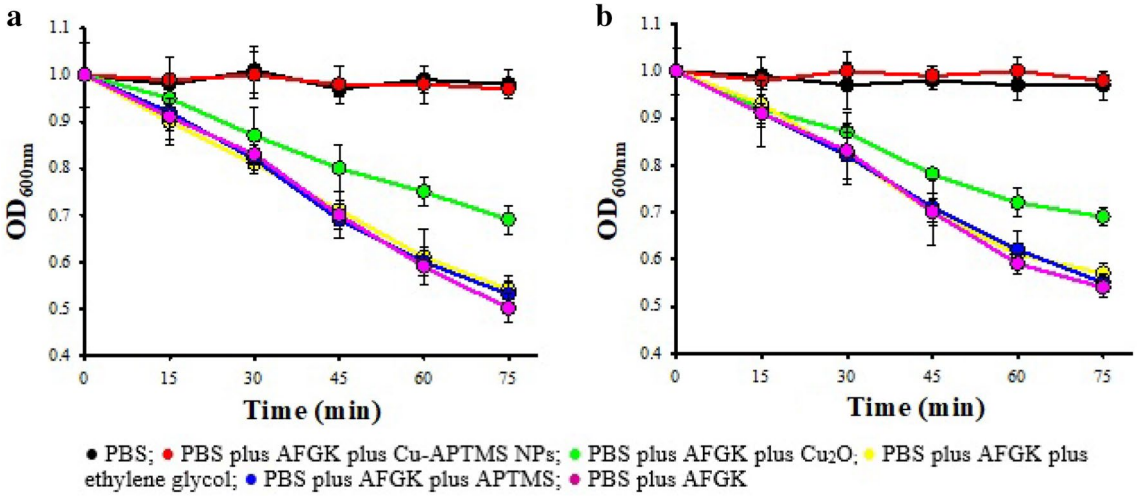

Fig. 7 Anti-germinative activity of Cu-APTMS NPs on bacterial spores. The inhibition of germination of *B. subtilis* spores (**a**) and *C. perfringens* spores (**b**) with Cu-APTMS in ethylene glycol (red circle) or Cu_2O in water (green circle) at a concentration of 80 µM was evaluated in a PBS buffer supplemented with the AFGK germinant mixture at room temperature. The figure also shows the germination rate of spores resuspended in the PBS buffer plus: none (black circle), AFGK (pink circle), AFGK + ethylene glycol (yellow circle), and AFGK + APTMS (blue circle). Spore germination was measured by monitoring the decrease of the OD_{600nm} over time and confirmed by the loss of spore refractability. Experiments were performed in triplicate and a typical result ± S.E.M. is shown

siloxane groups was achieved. This fact favors the incorporation of the particles into solid inorganic matrices (SiO_2, TiO_2, etc.), allowing the manufacture of composite materials as films or powders to be used in technological applications.

Due to the high tendency of copper to oxidize, it is significant to have achieved stable copper nanoparticle systems. This allows for both the storage and handling of samples in air for their physicochemical characterization and also for biological or other applications. Moreover, this shows that the effectiveness of APTMS as capping agent is as good as that of other more common compounds such as PVP.

The microbicidal behavior of the Cu-APTMS NPs suspensions was verified, showing greater efficiency than copper (I) oxide. The inhibition of growth and lethal effects against Gram-positive, Gram-negative, yeast and molds were analyzed and the obtained results showed that the Cu-APTMS NPs were efficient microbicides at similar or lower concentrations than previously reported for other Cu-based microbicide preparations.

Acknowledgements The authors thank the Consejo Nacional de Investigaciones Científicas y Técnicas (CONICET, PIP-2013-0553) and the Agencia Nacional de Promoción Científica y Tecnológica (ANPCyT, PICT 20103-423 and PICT 2012-2577) for the financial support. We also thank Dra. Renata Strubbia for the assistance in acquiring the TEM images and Dr. Nestor Delorenzi for the use of the zeta potential analizer.

References

1. S. Guo, E. Wang, Noble metal Nanomaterials: controllable synthesis and application in fuel cells and analytical sensors. Nano Today **6**, 240–264 (2011)
2. Y. Yan, S.C. Warren, P. Fuller, B.A. Grzybowski, Chemoelectronic circuits based on metal nanoparticles. Nat. Nanotechnol. **11**, 603–608 (2016)
3. R.A. Potyrailo, Toward high value sensing: monolayer-protected metal nanoparticles in multivariable gas and vapor sensors. Chem. Soc. Rev. **46**, 5311–5346 (2017)
4. C. Shen, C. Hui, T. Yang, C. Xiao, J. Tian, L. Bao, S. Chen, H. Ding, H. Gao, Monodisperse noble-metal nanoparticles and their surface enhanced raman scattering properties. Chem. Mater. **20**, 6939–6944 (2008)
5. G. Prieto, J. Zecevic, H. Friedrich, K. Jong, P. Jongh, Towards stable catalysts by controlling collective properties of supported metal nanoparticles. Nat. Mater. **12**, 34–39 (2013)
6. B. Roldan Cuenya, Synthesis and catalytic properties of metal nanoparticles: size, shape, support, composition, and oxidation state effects. Thin Solid Films **518**, 3127–3150 (2010)
7. S.M. Dizaj, F. Lotfipoura, M. Barzegar-Jalali, M.H. Zarrintana, K. Adibkiab, Antimicrobial activity of the metals and metal oxide nanoparticles. Mater. Sci. Eng. C **44**, 278–284 (2014)
8. F. Parveen, B. Sannakki, M. Mandke, H. Pathan, Copper nanoparticles: synthesis methods and its light harvesting performance. Solar Energy Mater. Solar Cells **144**, 371–382 (2016)
9. D. Deng, Y. Jin, Y. Cheng, T. Qi, F. Xiao, Copper nanoparticles: aqueous phase synthesis and conductive films fabrication at low sintering temperature. ACS Appl. Mater. Interfaces **5**, 3839–3846 (2013)
10. S. Jeong, S.H. Lee, Y. Jo, S.S. Lee, Y. Seo, B. Ahn, G. Kim, G. Jang, J. Park, B. Ryu, Y. Choi, Air-stable, surface-oxide free Cu nanoparticles for highly conductive Cu ink and their application to printed graphene transistors. J. Mater. Chem. C. **1**, 2704–2710 (2013)

11. Y. Guo, F. Cao, X. Lei, L. Mang, S. Cheng, J. Song, Fluorescent copper nanoparticles: recent advances in synthesis and applications for sensing metal ions. Nanoscale **8**, 4852–4863 (2016)
12. T. Ramani, K. Prasant, B. Sreedhar, Air stable colloidal copper nanoparticles: synthesis, characterization and their surface-enhanced Raman scattering properties. Phys. E **77**, 65–71 (2016)
13. M. Gawande, A. Goswami, F. Felpin, T. Asefa, X. Huang, R. Silva, X. Zou, R. Zborl, R. Varma. Cu and Cu-based nanoparticles: synthesis and applications in catalysis. Chem. Rev. **116**, 3722–3811 (2016)
14. T. Kruk, K. Szczepanowicz, J. Stefanska, R. Socha. P. Warszynski, Synthesis and antimicrobial activity of monodisperse copper nanoparticles. Colloids Surf. B **128**, 17–22 (2015)
15. L. Duran Pachon, G. Rothenberg, Transition-metal nanoparticles: synthesis, stability and the leaching issue. Appl. Organometal. Chem. **22**, 288–299 (2008)
16. T. Dang-Bao, C. Pradel, I. Favier, M. Gómez, Making copper(0) nanoparticles in glycerol: a straightforward synthesis for a multipurpose catalyst. Adv. Synth. Catal. **359**, 2832–2846 (2017)
17. B.H. Patel, M.Z. Channiwala, S.B. Chaudhari, A.A. Mandot, Biosynthesis of copper nanoparticles; its characterization and efficacy against human pathogenic bacterium. J. Environ. Chem. Eng. **4**, 2163–2169 (2016)
18. L. Esteban-Tejeda, F. Malpartida, A. Esteban-Cubillo, C. Pecharromán, J.S. Moya. Antibacterial and antifungal activity of a soda-lime glass containing copper nanoparticles. Nanotechnology. **20**, 505701 (2009)
19. Y.W. Baek, Y.J. An, Microbial toxicity of metal oxide nanoparticles (CuO, NiO, ZnO and Sb_2O_3) to *Escherichia coli, Bacillus subtilis* and *Streptococcus aureus*. Sci. Total Envirom. **409**, 1603–1608 (2011)
20. A. Azam, A.S. Ahmed, M. Oves, M.S. Khan, A. Memic, Size-dependent antimicrobial properties of CuO nanoparticles against Gram-positive and -negative bacterial strains. Int. J. Nanomed. **7**, 3527–3535 (2012)
21. A.K. Chatterjee, R.K. Sarkar, A.P. Chattopadhyay, P. Aich, R. Chakraborty, T. Basu, A simple robust method for synthesis of metallic copper nanoparticles of high antibacterial potency against *E. coli*. Nanotechnology. **23**, 085103 (2012)
22. M.S. Hassan, T. Amna, O.B. Yang, M.H. El-Newehy, S.S. Al-Deyab, M.S. Khil. Smart copper oxide nanocrystals: synthesis, characterization, electrochemical and potent antibacterial activity. Colloids Surf. B. Biointerfaces. **97**, 201–206 (2012)
23. A. Pramanik, D. Laha, D. Bhattacharya, P. Pramanik, P. Karmakar, A novel study on antibacterial activity of copper iodide nanoparticles mediated by DNA and membrane damage. Colloids Surf. B. Biointerfaces. **96**, 50–55 (2012)
24. K. Giannousi, K. Lafazanis, J. Arvanitidis, A. Pantazaki, C. Dendrinou-Samara, Hydrothermal synthesis of copper based nanoparticles: antimicrobial screening and interaction with DNA. J. Inorg. Biochem. **133**, 24–32 (2014)
25. D. Yohan, D. Chithrani, Applications of nanoparticles in nanomedicine. J. Biomed. Nanotechnol. **10**, 2371–2392 (2014)
26. T.V. Duncan, Applications of nanotechnology in food packaging and food safety: barrier materials, antimicrobials and sensors. J. Colloid Interface Sci. **363**, 1–24 (2011)
27. J.A. Lemire, J.J. Harrison, S.P. Turner, Antimicrobial activity of metals, mechanisms, molecular targets and applications. Nat. Rev. Microbiol. **11**, 371–384 (2016)
28. A. Stacy, L. McNally, S.E. Darch, S.P. Brown, M. Whiteley, The biogeography of polymicrobial infection. Nat. Rev. Microbiol. **14**, 93–105 (2016)
29. A.N. Kremer, H.J. Hoffmann, Substractive hybridization yields a silver resistance determinant unique to nosocomial pathogens in the *Enterobacter cloacae* complex. J. Clin. Microbiol. **50**, 3249–3257 (2012)
30. L.L. Maragakis, E.N. Perencecich, S.E. Cosgrove, Clinical and economic burden of antimicrobial resistance. Expert Rev. Anti-Infect. Ther. **5**, 751–763 (2008)
31. A. Alanis, Resistance to antibiotics: are we in the post-antibiotic era? Arch. Med. Res. **36**, 697–705 (2005)
32. R. Laxminarayan, A. Duse, C. Wattal, A.K.M. Zaidi, F. Heiman, L. Wertheim, N. Sumpradit, E. Vlieghe et al., Antimicrobial resistance the need for global solutions. Lancet Inf. Dis. **12**, 1057–1098 (2013)
33. T.D. Gootz, The global problem of antibiotic resistance. Crit. Rev. Immunol. **30**, 79–93 (2010)
34. CDC, *Antibiotic resistance threats in the United States* (Center for Disease Control and Prevention, Atlanta, 2013)
35. U. Theuretzbacher, Antibiotic innovation for future public health needs. Clin. Microbiol. Infect. **23**, 713–717 (2017)
36. S. Rossiter, M. Fletcher, W. Wuest, Natural products as platforms to overcome antibiotic resistance. Chem. Rev. **117**, 12415–12474 (2017)
37. V. Challinor, H. Bode, Bioactive natural products from novel microbial sources. Ann. NY. Acad. Sci. **1354**, 82–97 (2015)
38. T. Rahman, B. Yarnall, D. Doyle, Efflux drug transporters at the forefront of antimicrobial resistance. Eur. Biophys. J. **46**, 647–653 (2017)
39. S. Correia, P. Poeta, M. Hébraud, J.L. Capelo, G. Igrejas, Mechanisms of quinolone action and resistance: where do we stand? J. Med. Microbiol. **66**, 551–559 (2017)
40. D. Dar, R. Sorek, Regulation of antibiotic-resistance by non-coding RNA in bacteria. Curr. Opin. Microbiol. **36**, 111–117 (2017)
41. N. Høiby, T. Bjarnsholt, M. Givskov, S. Molinc, O. Ciofub, Antibiotic resistance of bacterial biofilms. Int. J. Antimicrob. Agent. **35**, 322–332 (2010)
42. A.K. Thabit, J.L. Crandon, D.P. Nicolau, Antimicrobial resistance: impact on clinical and economical outcomes and the need for new antimicrobials. Expert Opin. Pharmacother. **2**, 159–177 (2015)
43. J.N. Slavin, J. Asnis, U.O. Häfeli, H. Bach, Metal nanoparticles: understanding the mechanisms behind antibacterial activity. J. Nanobiotechnol. **15**, 65 (2017)
44. F.N. Oktar, M. Yetmez, D. Ficai, A. Ficai, F. Dumitru, A. Pica, Molecular mechanisms and targets of the antimicrobial activity of metal nanoparticles. Curr. Top. Med. Chem. **15**, 1583–1588 (2015)
45. L. Wang, C. Hu, L. Shao, The antimicrobial activity of nanoparticles: present situation and prospects for the future. Int. J. Nanomed. **12**, 1227–1249 (2017)
46. G.R. Rudamurthy, M.K. Swamy, U.R. Sinniah, A. Ghasemzadeh, Nanoparticles: alternatives against drug-resistant pathogenic microbes. Molecules **21**, 836 (2016)
47. M. Vincent, R.E. Duval, P. Hartemann, M. Engels-Deutsch, Contact killing and antimicrobial properties of copper. J. Appl. Microbiol. **124**, 1032–1046 (2017)
48. H. Palza, M. Nuñez, R. Bastías, K. Delgado, In situ antimicrobial behavior of materials with copper-based additives in a hospital environment. Int. J. Antimicrob. Agents **51**, 912–917 (2018)
49. T.M. Dung Dang, T.T. Tuyet Le, E. Fribourg-Blanc, M. Chien Dang, The influence of solvents and surfactants on the preparation of copper nanoparticles by a chemical reduction method. Adv. Nat. Sci. Nanosci. Nanotechnol. **2**, 025004 (2011)
50. P. Singh, Y. Kim, D. Zhang, D. Yang, Biological synthesis of nanoparticles from plants and microorganisms. Trends Biotechnol. **34**, 588–599 (2016)
51. N. Pantidos, M.C. Edmundson, L. Horsfall, Room temperature bioproduction, isolation and anti-microbial properties of stable

elemental copper nanoparticles. New Biotechnol. **40**, 275–281 (2018)
52. N. Nagar, V. Devra, Green synthesis and characterization of copper nanoparticles using *Azadirachta indica* leaves. Mater. Chem. Phys. **213**, 44–51 (2018)
53. N. Sreeju, A. Rufus, D. Philip, Microwave–assisted rapid synthesis of copper nanoparticles with exceptional stability and their multifaceted applications. J. Mol. Liq. **221**, 1008–1021 (2016)
54. G.H. Hong, S.W. Kang, Synthesis of monodisperse copper nanoparticles by utilizing 1-butyl-3-methylimidazolium nitrate and its role as counteranion in ionic liquid in the formation of nanoparticles. Ind. Eng. Chem. Res. **52**, 794–797 (2013)
55. C. Schmadicke, M. Poetschke, L.D. Renner, L. Baraban, M. Bobeth, G. Cuniberti, Copper nanowire synthesis by directed electrochemical nanowire assembly. RSC Adv **4**, 46363–46368 (2014)
56. M.H. Kang, S.J. Lee, J.Y. Park, J.K. Park, Carbon-coated copper nanoparticles: Characterization and fabrication via ultrasonic irradiation. J. Alloys Compd. **735**, 2162–2166 (2018)
57. A.R. Sadrolhosseini, A.S.B.M. Noor, K. Shameli, G. Mamdoohi, M.M. Moksin, M.A. Mahdi, Laser ablation synthesis and optical properties of copper nanoparticles. J. Mater. Res. **28**, 2629–2636 (2013)
58. A. Kumar, A. Saxena, A. De, R. Shankar, S. Mozumdar, Facile synthesis of size-tunable copper and copper oxide nanoparticles using reverse microemulsions. RSC Adv. **3**, 5015–5021 (2013)
59. A. Wang, L. Chen, F. Xu, Z. Yan, In-situ synthesis of copper nanoparticles within ionic liquid–in—vegetable oil microemulsions and their direct use as high efficient nanolubricants. RSC Adv. **4**, 45251–45257 (2014)
60. L. Xu, J.H. Peng, C. Srinivasakannan, L.B. Zhang, D. Zhang, C. Liu, S.X. Wang, A.Q. Shen. Synthesis of copper nanoparticles by a T-shaped microfluidic device. RSC Adv. **4**, 25155–25159 (2014)
61. Q. Liu, D. Zhou, Y. Yamamoto, R. Ichino, M. Okido, Preparation of Cu nanoparticles with NaH4 by aqueous reduction method. Trans. Nonferrous Met. Soc. China **22**, 117–123 (2012)
62. K. Liu, Y. Song, S. Chen, Electrocatalytic activities of alkyne-functionalized copper nanoparticles in oxygen reduction in alkaline. Media. J. Power Sources **268**, 469–475 (2014)
63. Y. Hokita, M. Kanzaki, T. Sugiyama, R. Arakawa, H. Kawasaki, High-concentration synthesis of sub-10-nm copper nanoparticles for application to conductive nanoinks. ACS Appl. Mater. Interfaces **7**, 19382–19389 (2015)
64. H.X. Zhang, U. Siegert, R. Liu, W.B. Cai. Facile fabrication of ultrafine copper nanoparticles in organic solvent. Nanoscale Res. Lett. **4**, 705–708 (2009)
65. B.K. Park, S. Jeong, D. Kim, J. Moon, S. Lim, J.S. Kim, Synthesis and size control of monodisperse copper nanoparticles by polyol method. J. Coll. Interface Sci. **311**, 417–424 (2007)
66. M.V. Roldán, P. de Oña, Y. Castro, A. Durán, P. Faccendini, C. Lagier, R. Grau, N.S. Pellegri, Photocatalytic and biocidal activity of novel coating systems of mesoporous and dense TiO2-anatase containing silver nanoparticles. Mater. Sci. Eng. C **43**, 630–640 (2014)
67. M.V. Roldán, Y. Castro, N. Pellegri, A. Durán, Enhanced photocatalytic activity of mesoporous TiO2 Sol-Gel coatings doped with Ag nanoparticles. J. Sol-Gel Sci. Technol. **76**, 180–194 (2015)
68. C. Rodriguez-Abreu, M. Sánchez-Domínguez, *Nanocolloids: A Meeting Point for Scientists and Technologists*, 1st edn. (Elsevier, 2016), pp. 159
69. L. Liz-Marzán, M. Giersig, P. Mulvaney, Synthesis of gold-silica core-shell particles. Langmuir. No. 18 **12**, 4329–4335 (1996)
70. P. Pongwan, K. Wetchakun, S. Phanichphan, N. Wetchakun, Enhancement of visible-light photocatalytic activity of Cu-doped TiO2 nanoparticles. Res. Chem. Intermed. **42**, 4 (2015)
71. X.-M. Zhu, Y.-X.J. Wang, K.C.-F. Leung, S.-F. Lee, F. Zhao, D.-W. Wang, J.M. Lai, C. Wan, C.H. Cheng, A.T. Ahuja, Enhanced cellular uptake of aminosilane-coated superparamagnetic iron oxide nanoparticles in mammalian cell lines. Int. J. Nanomed. **7**, 953–964 (2012)
72. A.L. Arabolaza, A. Nakamura, M.E. Pedrido, L. Martelotto, L. Orsaria, R.R. Grau. Characterization of a novel inhibitory feeback of the anti-anti-sigma SpoIIA on Spo0A activation during development in *Bacillus subtilis*. Mol. Microbiol. **47**, 1251–1263 (2003)
73. M.B. Méndez, A. Goñi, W. Ramirez, R.R. Grau. Sugar inhibits the production of the toxins that trigger clostridial gas gangrene. Microb. Pathog. **52**, 85–91 (2012)
74. R. Grau, D. Gardiol, G.C. Glikin, D. de Mendoza, DNA supercoiling and thermal regulation of unsaturated fatty acid synthesis in *Bacillus subtilis*. Mol. Microbiol. **11**, 933–941 (1994)
75. V.A. Philippe, M.B. Méndez, I.H. Huang, L.M. Orsaria, M.R. Sarker, R.R. Grau. Inorganic phosphate induces spore morphogenesis and enterotoxin production in the intestinal pathogen *Clostridium perfringens*. Infect. Immun. **74**, 3651–3656 (2006)
76. T. Igarashi, P. Setlow, Interaction between individual protein components of the GerA and GerB nutrient receptors that trigger germination on *Bacillus subtilis* spores. J. Bacteriol. **187**, 2514–2518 (2005)
77. D.V. Ravi Kumar, I. Kim, Z. Zhong, K. Kim, D. Lee, J. Moon, Cu(II)-alkyl amine complex mediated hydrothermal synthesis of Cu nanowires: exploring the dual role of alkyl amines. Phys. Chem. Chem. Phys. **16**, 22107 (2014)
78. K. Rice, A. Paterson, M. Stoykovich, Nanoscale Kirkendall effect and oxidation kinetics in copper nanocrystals characterized by real-time, in situ optical spectroscopy, Part. Part. Syst. Charact. **32**, 1–8 (2014)
79. L. Lutterotti, Total pattern fitting for the combined size-strain-stress-texture determination in thin film diffraction. Nuclear Inst. Methods Phys. Res. B **268**, 334–340 (2010)
80. C. Salzemann, A. Brioude, M.-P. Pileni, Tuning of copper nanocrystals optical properties with their shapes. J. Phys. Chem. B **110**, 7208–7212 (2006)
81. S. Bhattacharjee, DLS and zeta potential-What they are and what they are not? J. Control. Release **235**, 337–351 (2016)
82. G. Socrates, *Infrared and Raman Characteristic Group Frequencies*, 3rd. edn. (John Wiley & Sons Ltd., Chichester, 2001), p. 145
83. L. Téllez, F. Rubio, R. Peña-Alonso, J. Rubio, Seguimiento por espectroscopia infrarroja (FT-IR) de la copolimerización de TEOS (tetraetilortosilicato) y PDMS (polidimetilsiloxano) en presencia de tbt (tetrabutiltitanio). Bol. Soc. Esp. Ceram. **43**, 883–890 (2004)
84. M.V. Roldán, N.S. Pellegri, O.A. de Sanctis, Optical response of silver nanoparticles stabilized by amines to LSPR based sensors. Proc. Mater. Sci. **1**, 594–600 (2012)
85. R.C. Rodríguez, L. Yate, E. Coy, ÁM. Martínez-Villacorta, A.V. Bordonia, S. Moya, P.C. Angelomé, Copper nanoparticles synthesis in hybrid mesoporous thin films: controlling oxidation state and catalytic performance through pore chemistry. Appl. Surf. Sci. **471**, 862–868 (2019)
86. V. Donato, F. Rodríguez Ayala, S. Cogliati, C. Bauman, J.G. Costa, C. Leñini, R. Grau, *Bacillus subtilis* biofilm extends *Caenorhabditis elegans* longevity through downregulation of the insulin-like signaling pathway. Nat Commun. **8**, 14332 (2017)
87. M. Mendez, I. Huang, K. Ohtani, R. Grau, T. Shimizu, M.R. Sarker, Carbon catabolite repression of type IV pilus-dependent gliding motility in the anaerobic pathogen *Clostridium perfringens*. J. Bacteriol. **190**, 48–60 (2008)
88. J.M. Rangel, P.H. Sparling, C. Crowe, P.M. Griffin, D.L. Swerdlow, Epidemiology of *Escherichia coli* O157:H7 outbreaks,

United States, 1982–2002. Emerg. Infect. Dis. **11**, 603–609 (2005)
89. J.A. Vázquez-Boland, M. Kuhn, P. Berche, T. Chakraborty, G. Domínguez-Bernal, W. Goebel, B. González-Zorn, J. Wehland, J. Kreft, *Listeria* pathogenesis and molecular virulence determinants. Clin. Microbiol. Rev. **14**, 584–640 (2001)
90. Y.D. Bakthavatchalam, L.E. Nabarro, B. Veeraraghavan, Evolving rapid methicillin-resistant *Staphylococcus aureus* detection: cover all the bases. J. Glob. Infect. Dis. **9**, 18–22 (2017)
91. A.K. Chatterjee, R. Chakraborty, T. Basu, Mechanism of antibacterial activity of copper nanoparticles. Nanotechnology **25**, 135101 (2014)
92. T. Maniatis, E.F. Fritsch, J. Sambrook. Molecular cloning: a laboratory manual. (Cold Spring Harbor Laboratory, New York, 545, 1982). ISBN 0-87969-136-0
93. A. Bonici, G. Lusvardi, G. Malavasi, L. Menabue, A. Piva, Synthesis and characterization of bioactive glasses functionalized with Cu nanoparticles and organic molecules. J. Eur. Ceram. Soc. **32**, 2777–2783 (2012)
94. V. Ainaa, G. Cerrato, G. Martra, G. Malavasid, G. Lusvardid, L. Menabue, Towards the controlled release of metal nanoparticles from biomaterials: physico-chemical, morphological and bioactivity features of Cu-containing sol-gel glasses. Appl. Surf. Sci. **283**, 240–248 (2013)
95. S. Jadhav, S. Gaikwad, M. Nimse, A. Rajbhoj, Copper oxide nanoparticles: synthesis, characterization and their antibacterial activity. J. Clust. Sci. **22**, 121–129 (2011)
96. M. Hans, A. Erbe, S. Mathews, Y. Chen, M. Solioz, F. Mücklich. Role of copper oxides in contact killing of bacteria. Langmuir **29**, 16160–16166 (2013)
97. O. Akhavan, E. Ghaderi, Cu and CuO nanoparticles immobilized by silica thin films as antibacterial materials and photocatalysts. Surf. Coat. Technol. **205**, 219–223 (2010)
98. S. Cogliati, J.G. Costa, F. Rodriguez Ayala, V. Donato, R. Grau, Bacterial spores and its relatives as agents of mass destruction. J. Bioterror. Biodef **7**, 141 (2016)
99. M.J. Leggett, G. McDonnell, S.P. Denyer, P. Setlow, J.Y. Maillard, Bacterial spore structures and their protective role in biocide resistance. J. Appl. Microbiol. **113**, 485–498 (2012)

Publisher's Note Springer Nature remains neutral with regard to jurisdictional claims in published maps and institutional affiliations.